Physica A 389 (2010) 825–836

Contents lists available at ScienceDirect

Physica A

journal homepage: www.elsevier.com/locate/physa

Explaining traffic patterns at on-ramp vicinity by a driver perception model in the framework of three-phase traffic theory

Shuyan He, Wei Guan*, Liying Song

MOE Key Laboratory for Urban Transportation Complex System Theory and Technology, Beijing Jiaotong University, China

ARTICLE INFO

Article history:
Received 18 March 2009
Received in revised form 5 September 2009
Available online 17 October 2009

Keywords:
Traffic flow model
Driving behavior
Driver perception
Numerical simulation
Urban freeway

ABSTRACT

In traffic system, driving behaviors change with the surrounding traffic perceived by drivers, resulting in the complex spatio-temporal traffic patterns. Accordingly, in the majority of traffic models, vehicle accelerations are described by dynamic equations based on driving behavior, system dynamics and some underlying steady-state velocity-gap (bumper-to-bumper spacing) relation in order to guarantee the realistic human behavior. This paper proposes a deterministic car-following model based on a multi-branch fundamental diagram with each branch representing a particular category of driving style. Furthermore, an additional dynamic perception equation is introduced to reflect the driving style adaptation in response to the change in surrounding traffic situations. With simulation based on the proposed "driver perception model" (DP model), empirical findings of traffic breakdown and observed spatio-temporal patterns at on-ramp vicinity are reproduced. Furthermore, comparison results show the consistency between numerical simulation and the real traffic data of Beijing urban freeway.

1. Introduction

1.1. Literature review

In traffic system, driver behaviors are generally generated from several driving motivations, including efficiency, safety, comfort, fuel economy etc. Competition among different desires, along with the physical restrictions and psychological factors, produces complex traffic phenomena. The fundamental feature of traffic flow is the velocity–density (velocity–gap) relationship which reflects aggregated human behaviors. In the majority of traffic flow models, the steady-state solution, also named as "fundamental diagram", assumes a similar shape of average measured data. To date, various forms of fundamental diagrams and their related dynamic equations have been proposed by means of various traffic models to reproduce the observed traffic phenomena.

The functional form of fundamental diagram was firstly proposed as a deterministic function calibrated from empirical data [1,2]. However, most of the fundamental diagrams were derived from steady-state solutions of a microscopic model [3,4] or functions restricted to some critical constraints [5] based on some behavioral and theoretical foundation. These classical forms of fundamental diagrams are characterized by a quasi-linear free flow branch and a monotonically decreased branch representing congested flow in the flow-density plane. Those models are capable of representing free flow and stop-and-go traffic to a certain extent. But some of them failed to reproduce the hysteresis effect or the "synchronized flow" with a finite velocity observed at a moderate density, which is characterized by the observed synchronized traffic states among lanes [6–8]. Thus further improvements on traffic modeling require more complicated descriptions of dynamic system behavior and more realistic forms of fundamental diagram or both of them.

* Corresponding author.
E-mail address: weig@center.njtu.edu.cn (W. Guan).

0378-4371/$ – see front matter © 2009 Elsevier B.V. All rights reserved.
doi:10.1016/j.physa.2009.10.014

Dynamic system behaviors are improved by considering more sophisticated human behaviors in recent works. Such as anticipation, memory effect, heterogeneities of drivers/vehicles or multi-lane interactions. In Refs. [3,9], anticipation is related to velocity difference between two successive vehicles. In Ref. [10], driver reaction on breaking light of front vehicle is considered. In Ref. [11], instead of considering space gap to immediate preceding vehicle, weighted gap of several preceding vehicles is integrated in an optimal velocity function. Real driver behavior that reflects driver perception to past traffic situation is modeled as a memory effect in Refs. [12–14], where a critical time gap T is adjusted by the surrounding traffic situations such as velocity and velocity deviation. Heterogeneities and multi-lane vehicle interactions are realistic approximations to real traffic. In Ref. [15], different driver behaviors of "rabbit" and "slug" are modeled as main reason for capacity drop and synchronization among lanes. In Ref. [16], widely scattered flow-density data are reproduced by a relaxation of time headway through lane changes in multi-lane traffic.

Apart from reproducing complex traffic patterns through modification on dynamic system behaviors, fundamental diagrams are supposed to incorporate multi-phase features in nature. In Ref. [17], the phase transition was explained as the change of time gap found on the proposed flow-density diagrams with multiple branches. A fundamental diagram with multiple turning points corresponding to multiple phases are introduced in Ref. [18]. The hysteresis effect is modeled in Ref. [19] through a phase-dependent time gap variation in a steady-state velocity–gap function. On a macroscopic level, the additional equilibrium velocities located at the high flow branch and the jam line are generated by the balanced vehicular traffic model(BVT model), reproducing traffic patterns observed in front of bottlenecks [20].

Differently, models based on Kerner's three-phase traffic theory [21,22] follow different behavior hypothesis that a driver accepts a range of different hypothetical steady states with space gaps at the same vehicle speed in synchronized flow, i.e., steady states of synchronized flow cover a 2D region in the flow-density plane. Microscopic models proposed in Refs. [21,22] reproduce empirical phases of free flow, synchronized flow and wide moving jam, as well as complex traffic patterns related to first-order phase transitions of free flow to synchronized flow (F $\Rightarrow$ S) and synchronized flow to wide moving jam (S $\Rightarrow$ J), which are not supported in fundamental diagram approaches.

1.2. Results and hypotheses of Kerner's three-phase traffic theory used in the driver perception model

In Kerner's three-phase traffic theory, there are three traffic phases, free flow (F), synchronized flow (S), and wide moving jam (J). The wide moving jam and synchronized flow phases are defined through empirical criteria related to spatio-temporal features of these different traffic phases. A wide moving jam is a moving jam that maintains the mean velocity of the downstream jam front, even when the jam propagates through any other traffic states or freeway bottlenecks. In contrast, the downstream front of the "synchronized flow" phase is often fixed at a freeway bottleneck. Within this front vehicles accelerate from lower speeds in synchronized flow to higher speeds in free flow [21]. Wide moving jams emerge spontaneously due to a sequence of F $\Rightarrow$ S and S $\Rightarrow$ J transitions.

This paper proposes a "driver perception model" (DP model) to describe the traffic at inhomogeneity vicinity in the framework of three-phase traffic theory. The model is a deterministic, time continuous car-following model of single-lane traffic with identical vehicles. The so-called "driver perception" is originated from a driving-behavior adaptation rule based on past traffic situation a driver has perceived. In this paper, a "perception distance" d_c is introduced to characterize the driving styles. Similar to the critical time headway T in Refs. [12,13], d_c is a character space gap to the preceding vehicle. As driving style changes with surrounding traffic, d_c is adapted temporally. According to three-phase traffic theory, if a vehicle cannot pass the preceding vehicle driving at a synchronized flow speed, the driver behavior within the 2D region of synchronized flow states is determined by the speed adaptation effect in synchronized flow. The adaption of d_c can be compared to the speed adaption rule implemented in models based on three-phase traffic theory [21].

With the multi-valued d_c, the main difference between DP model and models based on fundamental diagram approach is that the steady-state solution of DP model covers a 2D area in the flow-density plane. In term of the 2D region of steady states, the proposed DP model follows the hypothesis of three-phase traffic theory that the synchronized flow states cover a 2D region. Furthermore, the open boundary simulations based on DP model show different phases of free flow, synchronized flow and wide moving jam. Moreover, the sequenced phase transitions of F $\Rightarrow$ S and S $\Rightarrow$ J are also reproduced.

2. Introduction to driver perception model

2.1. Empirical evidence for multi-branch fundamental diagram

Fundamental diagram (FD) is usually an approximation of empirical flow-density relations. However, at different locations at inhomogeneity vicinity, flow-density relations show great deviations from each other. To describe the variety of FDs, a popular method is to derive FDs of each location independently. In a different way, the multi-branch fundamental diagram proposed in the DP model is originated from an integrated view on a number of different locations. Here three sections are illustrated here as examples to explain the empirical evidence for the multi-branch fundamental diagram.

Fig. 2 shows the flow-density relations at median lanes (solid circles) and shoulder lanes (white squares) at three sections during a morning peak. The road structure is in Fig. 1.

The flow-density relations show some empirical characters related to road inhomogeneity:

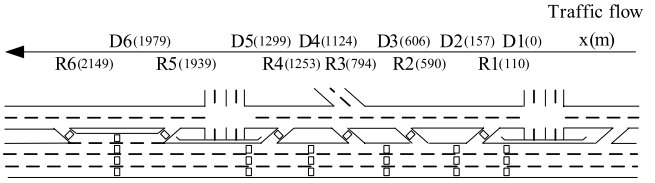

Fig. 1. Sketch diagram of a segment in Beijing 2nd ring road. D1–D6 are mainroad detectors and R1–R6 are ramp detectors.

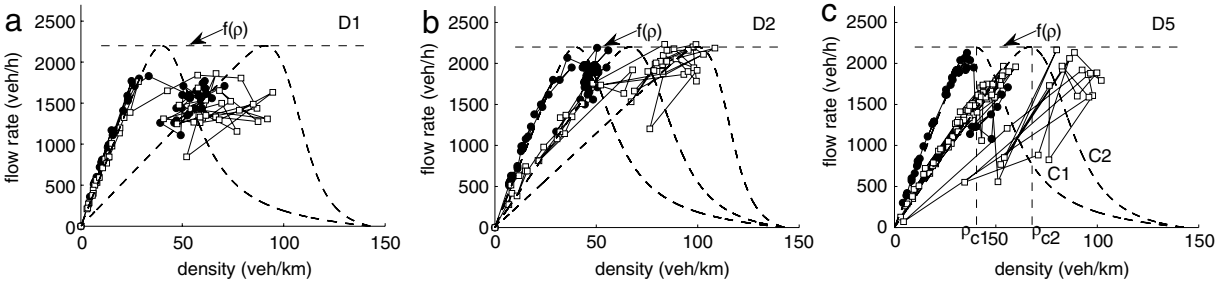

Fig. 2. Average two-min. flow-density data at three sections of Beijing urban freeway at morning peak (•: median lane; □: shoulder lane) on May 14, 2007. Dashed lines show the possible branches of fundamental diagram related to.

1. Free flow speed is sometimes lower than driver desired speed at inhomogeneity vicinity, such as the low density ($\leqslant$40 vpl/km) states of shoulder lanes in Fig. 2(b) and (c). In the researched urban freeway segment, with a speed limit of 80 km/h and identical lane using policy, lane free flow speeds are close to each other in most cases (see Fig. 2(a)). However, the balance will be destroyed at some location such as shoulder lane at on-ramp downstream where vehicles coming from on-ramp have not accelerated to a high speed within such a short distance yet.
2. Generally, free flow and congested flow at homogeneous road are divided by a velocity–gap as a result of traffic breakdown. In Fig. 2(a), free flow states form a quasi-linear line with positive slope at low density range while congested flow states locate at high density range without a certain shape. But in fact, the "free flow" with lower slope on the flow-density plane at road inhomogeneity (e.g. shoulder lane in Fig. 2(c)) is no longer free when density increases to a high value. Such state can be seen as a "quasi-free" state, or a "coherent moving" state mentioned in Refs. [23–25]. Moreover, in Fig. 2(c), the congested flow at median lane and the "quasi-free" flow at shoulder lane are partly overlapped. At this point, free flow and congested flow are just relative concepts corresponding to particular traffic environment. There is no clear separation between free flow and congested flow for all locations on one flow-density plane.
3. Two types of flow are observed. The first one is homogeneous flow. For example, in Fig. 2, all free flow states, "quasi-free" states and congested states except shoulder lane in (a) and (c) are homogeneous flow, which is characterized by stabilized and finite speed. The second type is stop-and-go traffic, such as congested flows in shoulder lanes in (a) and (c) where flows oscillate both on speed and flow rate. In Fig. 2(c), the states in jam is located close to the origin of the flow-density plane for the overestimated speed in the temporal averaged data.

The above empirical features give some implications on traffic modeling.

1. The first one is the derivation of fundamental diagram. In a fundamental diagram approach, there is a hypothetical equilibrium flow-density relation where free flow lies on low density with positive slope and congested flow on the part of negative slope. On the other hand, according to the above observation 2 and empirical data in Fig. 2(c), congested flow at D5 median lane could be treated as staying on a positive slope part of another equilibrium flow-density relation where free flow at D5 shoulder lane is realized. Analogously, all homogeneous flows can be represented in a similar form. In Fig. 2, dashed curves are approximated equilibrium flow-density relations, which is called a branch of fundamental diagram (FD branch for short) in DP model.
2. Based on the approximated FD branches, breakdowns from free flow to homogeneous congested flow can be modeled as a jump from one FD branch to another one.
3. Stop-and-go traffic is unstable where perturbation grows during propagation. In this case, positive and negative wave speeds coexist, indicating that flows reach negative slope part of FD branches. Shoulder lane in Fig. 2(c) is an example for stop-and-go traffic.

To derive branches of fundamental diagrams intuitively, firstly an universal density-dependent function of maximum flow rate $f(\rho_c)$ should be approximated in Fig. 2(b) and (c). Since $f(\rho_c)$ means the *maximum* flow rate ever observed at the entire road, it is not always necessary that flows at all locations reach this maximum value. Consequently $f(\rho_c)$ in Fig. 2(a) is higher than any flow-density points. Then dashed curves in Fig. 2 are drawn as approximated FD branches. Each FD branch can be characterized by a "perception density" ρ_c or a "perception distance" $d_c = 1/\rho_c - l$ (l is vehicle length), where

equilibrium flow rate Q_e reaches its maximum point. For example, with the constraint of maximum flow rate $f(\rho_c)$, the FD branches C1 and C2 in Fig. 2(c) are uniquely determined by perception densities ρ_{c1} and ρ_{c2}. As ρ_c is a continuous variable defines the domain of $f(\rho_c)$, there is an infinity number of FD branches in the proposed fundamental diagram.

The infinity number of fundamental diagram branches covers a 2D region of the flow-density plane, indicating that drivers accept a range of gaps at same speed. In the proposed driver perception model, gap at a certain moment is determined by the surrounding traffic situation that drivers have perceived. From such behavioral consideration, in the proposed fundamental diagram, every branch of the proposed fundamental diagram serves as a type of driving style.

2.2. Fundamental diagram of the driver perception model

Mathematically, it is assumed that a FD branch characterized by perception distance d_c is in the form of the widely used tanh function:

$$V_e(s, d_c) = m \cdot [\tanh(a \cdot s - b) + \tanh(b)] \tag{1}$$

or

$$Q_e(s, d_c) = \rho \cdot V_e(s, d_c) = \frac{1}{s + l} \cdot V_e(s, d_c), \tag{2}$$

where V_e and Q_e are equilibrium velocity and flow rate, s bumper-to-bumper gap, l the average vehicle length. Due to physical restriction, perception distance d_c is constrained to lie within the interval $[d_{\min}, d_{\max}]$. To reproduce the realistic flow-density relation, parameters m, a, b are functions of d_c which should be appropriately calibrated from empirical data. For unit consistency, m is in the unit same with V_e, i.e., m/s in this paper. Then b is in the unit of 1 while a in the unit of inverse of gap s, i.e., m^{-1} here.

The above analysis has shown that the equilibrium flow rate $Q_e(s, d_c)$ obtains its maximum value when $s = d_c$. Thus

$$\left.\frac{\partial Q_e(s, d_c)}{\partial s}\right|_{s=d_c} = 0. \tag{3}$$

Substitute Eq. (2) into Eq. (3), it gives

$$\left.\frac{\partial V_e(s, d_c)}{\partial s}\right|_{s=d_c} = \frac{1}{d_c + l} \cdot V_e(d_c) = Q_e(d_c) = g(d_c), \tag{4}$$

where g is an equivalent function to f with space gap s:

$$g(s) := f\left(\frac{1}{s + l}\right). \tag{5}$$

Substitute Eq. (1) into Eq. (4), the following two equations hold on:

$$\tanh(a \cdot d_c - b) + \tanh(b) = a(d_c + l) \cdot [1 - \tanh^2(a \cdot d_c - b)], \tag{6}$$

$$g(d_c) = \frac{m}{d_c + l}[\tanh(a \cdot d_c - b) + \tanh(b)]. \tag{7}$$

It is found that m is uniquely determined by d_c, a, b through Eq. (7) when the maximum flow rate $g(d_c)$ is provided. However, there is no unique solution for a, b according to Eqs. (6) and (7). Fig. 3(a) shows a solution surface for a and b as a function of d_c when $g(d_c)$ is supposed as a constant of 2200 veh/h. To obtain the explicit a and b, in this model, b is assumed as constant. Fig. 3(b) shows a solution for a when $b = 2$. Parameter m relates to the maximum velocity limit v_p that

$$v_p = \lim_{s \to +\infty} V_e(s, d_c) = m \cdot [1 + \tanh(b)]. \tag{8}$$

Fig. 3(b) also shows numerical solution for v_p when $b = 2$.

To conclude, the proposed fundamental diagram in DP model consists of a series of FD branches. Each branch is determined by a perception distance d_c and its corresponding maximum flow rate $g(d_c)$. The functional form and parameters are determined by Eqs. (1), (6) and (7).

2.3. Dynamic velocity equation

The dynamic velocity equation follows the form of OV model with limited acceleration:

$$\dot{v} = \min\{A, c \cdot [V_e(s, d_c) - v]\}, \tag{9}$$

where A represents the maximum acceleration. In Eq. (9), if d_c is a fixed, time-independent constant, the model behavior is the same as the well-known OV model. According to the previous research on OV model in Ref. [5], small perturbations will grow when $\mathrm{d}V_e/\mathrm{d}s > c/2$. In DP model, d_c is a time-dependent variable and the system stability is different with the OV model. However, the stability analysis with a fixed d_c still present some implications on the dynamic system behavior.

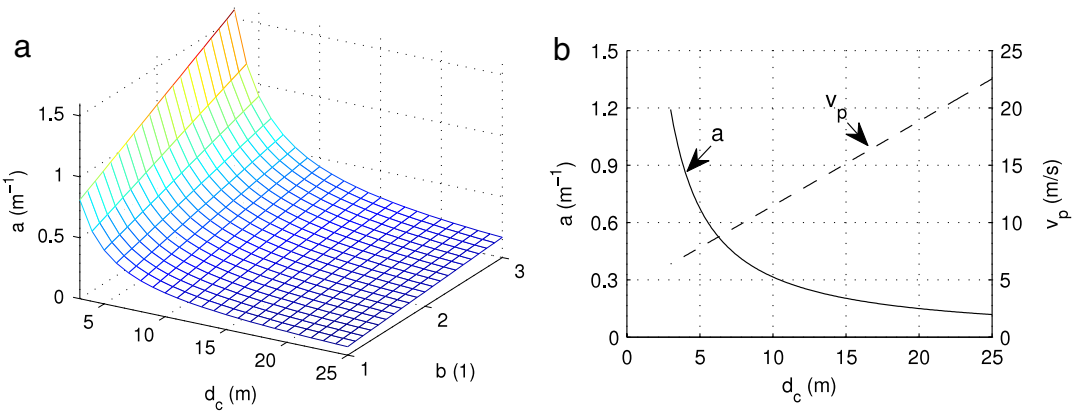

Fig. 3. (a) The numerical solution for a and b at different d_c; (b) The numerical solution for a and v_p at different d_c when $b = 2$ and $g(d_c) = 2200$ vpl/h.

2.4. Dynamic perception equation

The changes in driving style are modeled by transition between different perception curves. Since perception curve is only dependent on d_c, its evolution can be interpreted as a dynamic equation of d_c. In DP model, d_c changes without any explicit target value but only relate to the change rate of surrounding traffic situation. The empirical facts discussed in previous subsection show a decrease of d_c when breakdown occurs (see Fig. 2). Similarly, d_c will increase when traffic recovers. On the other hand, the phenomenon implies that a more cautious driving style will be adopted through a decrease of d_c when traffic become congested. Therefore a quantitative relationship between traffic state changes and driving style adaption is modeled by a dynamic perception equation

$$\dot{d_c} = \lambda(s, v) \cdot \Delta v. \tag{10}$$

In Eq. (10), $\Delta v = v_{pre} - v$ where v_{pre} is velocity of preceding vehicle. Δv is velocity difference between successive vehicles. Moreover, from equation $\Delta v = \dot{s}$, Δv is treated as a measurement for the change of the surrounding traffic situation. When $\Delta v < 0$, the space gap is decrease and the traffic gets more congested. Similarly, $\Delta v > 0$ indicates traffic gets free. λ is a state-dependent sensitive factor which measures driver's sensitiveness to the changes in the surrounding traffic situation. Normally, drivers are cautious when driving with low space gap to preceding vehicle or at high speed, indicating a more sensitive perception on the surrounding traffic. Consequently the amplitude of λ is supposed to decrease with the increasing space gap s and increase with the increasing velocity v.

Then the driver perception model will be solved by Eqs. (1), (9) and (10). However, the density-dependent maximum flow rate $f(\rho_c)$ or $g(s_c)$, model parameter c in Eq. (9) and λ in Eq. (10) need to be validated from real traffic data.

In accordance with the equilibrium velocity function equation (1), dynamic velocity function equation (9) and dynamic velocity equation (10), the steady states of DP model cover 2D region in flow-density plane. Indeed, as follows from Eq. (9), model steady states are given by formula $v = V_e(s, d_c)$, where $V_e(s, d_c)$ is a function of space gap s and also it depends on the parameter d_c (the perception distance). The dynamics of the perception distance d_c is described by Eq. (10). In steady state when speed difference $\Delta v = 0$, the parameter of d_c can take any values within the range $[d_{min}, d_{max}]$. As a result, the model steady states occupy the 2D region in speed-gap and flow-density planes. This 2D region is bounded by the curves $v = V_e(s, d_{min})$ and $v = V_e(s, d_{max})$ in speed-gap plane and the corresponding curves in flow-density plane. Moreover, the curve $v = V_e(s, d_{max})$ can be associated with the synchronization gap in Kerner's three-phase traffic theory, whereas the curve $v = V_e(s, d_{min})$ can be associated with the safe speed in the three-phase traffic theory. i.e., in the DP model the fundamental hypothesis of Kerner's theory has been incorporated.

As in Kerner's three-phase traffic theory, in the 2D region of synchronized flow states, a vehicle adapts its speed to the speed of the preceding vehicle — the speed adaptation effect. As in most other models based on three-phase traffic theory, the vehicle accelerates in DP model if it is slower than the preceding one and decelerates if it is faster than the preceding one (see, e.g., Ref. [22]). In DP model, there is the same speed adaptation effect at d_c within the range $[d_{min}, d_{max}]$: if speed difference $\Delta v \neq 0$, the value d_c varies according to Eq. (10) proportionally to Δv, this leads to the change in the parameter d_c in function $V_e(s, d_c)$ in Eq. (9), and as a result vehicle accelerates or decelerates in accordance with Eq. (9) until speed difference Δv becomes zero.

3. Model validation

In the field, the maximum flow rate appears at downstream of an on-ramp bottleneck as shown in Fig. 2(b). In shoulder lane, the maximum flow rate reaches 2200 vpl/h at high density because inserted vehicles from the on-ramp shortened time gap temporally. With thorough observations, the flow rates at other locations in the target area are not higher than the

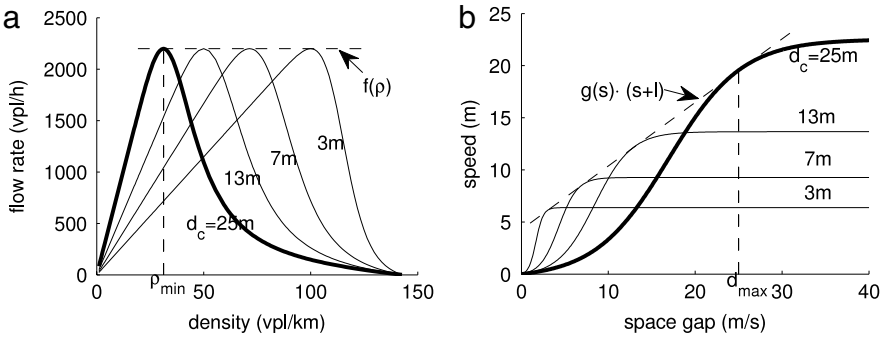

Fig. 4. Sample branches of fundamental diagram at (a) flow-density plane, (b) gap-speed plane.

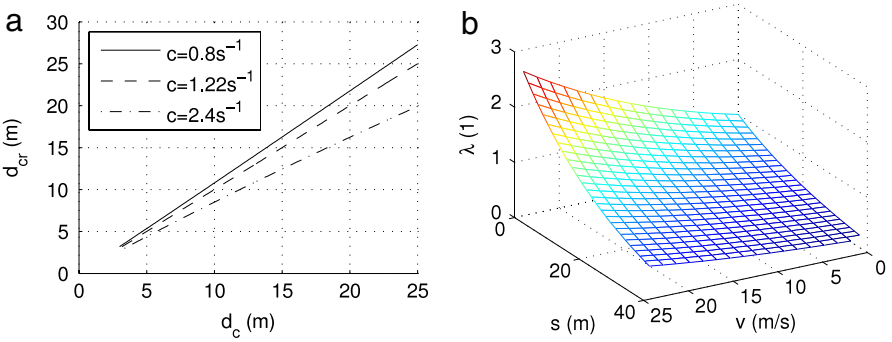

Fig. 5. (a) d_{cr} as a function of d_c under different c; (b) Sensitive factor λ as a function of v and s.

maximum flow rate shown in Fig. 2(b). Thus in the DP model, the maximum flow rate is approximated as $f(\rho)$ in Fig. 2(b) and (c), which could be assumed as a constant, i.e., $f(\rho_c) = g(s_c) = 2200$ vpl/h. However, the domain of s should within a valid range $[d_{\min}, d_{\max}]$ which can be approximated from empirical data. In this paper, $d_{\min} \approx 3$ m, $d_{\max} \approx 25$ m.

Given that $f(\rho_c) = 2200$ vpl/h, the multi-branch fundamental diagram is completely determined. Fig. 3(b) shows maximum speed v_p of each FD branch which is monotonically increased with perception distance d_c. Fig. 4 shows flow-density and speed-gap plane for several FD branches.

Parameter c and λ have to be seriously determined to reproduce the observed spatio-temporal patterns.

In DP model, the stability of a single FD branch is believed as the stability of the corresponding driving style. To analyze the stability of a particular driving style, d_c is assumed as a time-independent constant hence the DP model is then equivalent to OV model. In this case, the sensitive factor c in Eq. (9) is critical to system stability that the system is linearly unstable when $\mathrm{d}V_e(s, d_c)/\mathrm{d}s > c/2$. Then the critical distance d_{cr} is a function of perception distance d_c and satisfies $\mathrm{d}V_e(s, d_c)/\mathrm{d}s|_{s=d_{cr}} = c/2$. According to Eq. (4), if $c = 2 \cdot g(d_c)$, $\mathrm{d}V_e(s, d_c)/\mathrm{d}s = c/2 = g(d_c)$ is satisfied when $s = d_c$, that to say, the critical distance d_{cr} of FD branch d_c is exactly the perception distance d_c. It is also derived that when $c < 2 \cdot g(d_c)$, the critical distance d_{cr} is greater than d_c. Similarly, when $c > 2 \cdot g(d_c)$, $d_{cr} < d_c$. Fig. 5(a) shows the relationship between d_{cr} and d_c at different c when $f(\rho_c) = g(s_c) = 2200$ vpl/h $= 0.61$ vpl/s. It is found that when c is constant, d_{cr} increases with growing d_c, indicating a decreasing stability with growing d_c.

Parameter λ in Eq. (10) relates to system dynamic behavior. If $\lambda = 0$, d_c is constant and the DP model is identical to OV model. When $\lambda \neq 0$, complex system behavior is formed for the adaption of driving style through the change of d_c. Here λ is derived from driving desires for smooth and fast driving.

When traffic gets congested, i.e., $\Delta v < 0$ in Eq. (10), drivers will prefer to adopt a more stable driving style by a decreasing d_{cr} to avoid frequently stop-and-go behavior. Such a tendency is a result of drivers' desire for smooth moving. According to Fig. 5(a), the decreasing d_{cr} is realized by a decreasing d_c. However, when $\Delta v > 0$, drivers will prefer to a faster moving by a increasing v_p. This is a result of drivers' desire for fast moving. Fig. 3(b) shows numerical solutions for v_p as a function of d_c, it is found that the increasing v_p is realized by increasing d_c. With the form of $\dot{d}_c$ as Eq. (10), it is suggest that λ is a non-negative variable.

Previous discussion on Eq. (10) in Section 2 shows that $\lambda(s, v)$ decreases with increasing space gap s and increases with increasing velocity v for all legal v and s. Moreover, d_c should be constrained within a realistic range $[d_{\min}, d_{\max}]$.

Based on the above discussion, $\lambda(v, s)$ can be approximated by various function forms. Here an exponential form is used:

$$\lambda(v, s) = \begin{cases} 0 & d_c \geqslant d_{\max} \text{ and } \Delta v > 0 \\ 0 & d_c \leqslant d_{\min} \text{ and } \Delta v < 0 \\ \exp(\alpha \cdot v - \beta \cdot s) & \text{others.} \end{cases} \tag{11}$$

Table 1
Simulation parameters.

	Free flow Fig. 6(a), (b)	Homogeneous congestion Fig. 6(c), (d)	Stop-and-go traffic Fig. 6(e), (f)
$q_{(\text{main})}$ (vpl/h)	1422	1733	1657
$q_{(\text{on})}$ (vpl/h)	350	800	1300
$d_0^{(\text{up})}$ (m)	25	22	22
$d_0^{(\text{down})}$ (m)	25	22	22
$d_{\max}^{(\text{up})}$ (m)	25	25	25
$d_{\max}^{(\text{down})}$ (m)	25	25	25

Model with appropriate values of c, α and β should be able to reproduce homogeneous flow and stop-and-go flow as shown in Fig. 2. Simulations show that $c = 2.4\ \text{s}^{-1}$, $\alpha = 0.04\ \text{s/m}$ and $\beta = 0.04\ \text{m}^{-1}$ are suitable parameter sets. Fig. 5(b) shows λ at different v and s with the above α and β.

4. Simulated traffic patterns

Open boundary simulations are performed on a sufficient long one-lane road with an on-ramp of length L_r located at $x = 0$. Assume that the upstream boundary flow rate is $q_{(\text{main})}$ and downstream boundary vehicles freely leave the road during whole simulation process. Upstream and downstream may have different maximum perception distance $d_{\max}^{(\text{up})}$ and $d_{\max}^{(\text{down})}$, respectively. At $t = 0$, traffic flow at the whole road is initialized by $q_0 = q_{(\text{main})}$. At on-ramp upstream and downstream, initial perception distances are set to $d_0^{(\text{up})}$ and $d_0^{(\text{down})}$, respectively. On-ramp vehicles start entering mainroad at t_0 with a fixed flow rate $q_{(\text{on})}$. The on-ramp flow is persistent till the simulation process ends.

Vehicle from on-ramp will enter the mainroad between two successive vehicles with velocity v_r if the gap between the two vehicles is not less than g_r. v_r and g_r are given by

$$v_r = \min(v_0 \cdot r,\ v_{\text{pre}}), \tag{12}$$

$$g_r = l. \tag{13}$$

In Eq. (12), the term $v_0 \cdot r$ with $r < 1$ denotes the velocity limitation of the on-ramp. In Eq. (13), since l in the model already contains vehicle length and jam distance, the minimum gap g_r is equal to l. In the following simulation, L_r is set to be 400 m and $r = 0.8$.

At the bottleneck with one on-ramp, three typical spatio-temporal patterns, i.e., free flow (Fig. 6(a),(b)), synchronized flow (Fig. 6(c),(d)) and wide moving jam (Fig. 6(e),(f)), are shown in Fig. 6. The initial conditions for those three patterns are listed in Table 1.

Free flow pattern is shown in Fig. 6(a) and (b), both upstream and downstream are homogeneous flow. After on-ramp vehicles was inserted,downstream flow stays at FD branches with lower d_c and lower speed compared to the initial conditions. Although downstream speed slightly decreases, the congested state does not propagate upstream. Such pattern corresponds to the formation of high flow rate where speed is slightly lower than maximum speed and flow rate is close to maximum flow rate.

Synchronized flow is shown in Fig. 6(c) and (d), where traffic breakdown occurs at on-ramp vicinity and propagated upstream, generating a low speed homogeneous congested area. After on-ramp vehicles are inserted, the downstream flow first reaches high flow rate then stays at FD branches with a lower d_c compared to the initial state. Moreover, the congested flow propagates upstream, forming an area of synchronized flow. At on-ramp upstream, the corresponding perception distance almost reaches the minimum value, which is lower than downstream recovering flow.

Wide moving jam is shown in Fig. 6(e) and (f), where synchronized flow forms and propagates upstream firstly, then some perturbations grow and moving jams emerge finally. In Fig. 6(f), moving jam emerges from synchronized flow where $d_c = d_{\min}$. When vehicles escapes from jam, perception distance increases rapidly and free flow recovers.

As shown in Fig. 6, in accordance with Kerner's three-phase traffic theory and the phase definitions made in this theory the driver perception (DP) model developed in the paper exhibits three traffic phases. The wide moving jam and synchronized flow phases comply with the empirical criteria of synchronized flow and wide moving jam [21], respectively.

Moreover, the simulation results show two types of phase transitions. The phase transition from free flow to synchronized flow is realized through a breakdown of perception distance d_c. While during transition from synchronized flow to wide moving jam as shown in Fig. 6(f), perception distance remains constant because it reaches its minimum value $d_{\min}$. Thus when perturbation exceeds some critical density, it grows and forms jam finally. The reason for the sequence of F $\Rightarrow$ S and S $\Rightarrow$ J transitions is an "attraction" to boundaries of 2D region described in Ref. [22]. By doing this, the DP model describes the dynamics of F $\Rightarrow$ S and S $\Rightarrow$ J transitions postulated in three-phase traffic theory. This explains the result that wide moving jams emerge spontaneously due to a sequence of F $\Rightarrow$ S and S $\Rightarrow$ J transitions in accordance with three-phase traffic theory in the DP model.

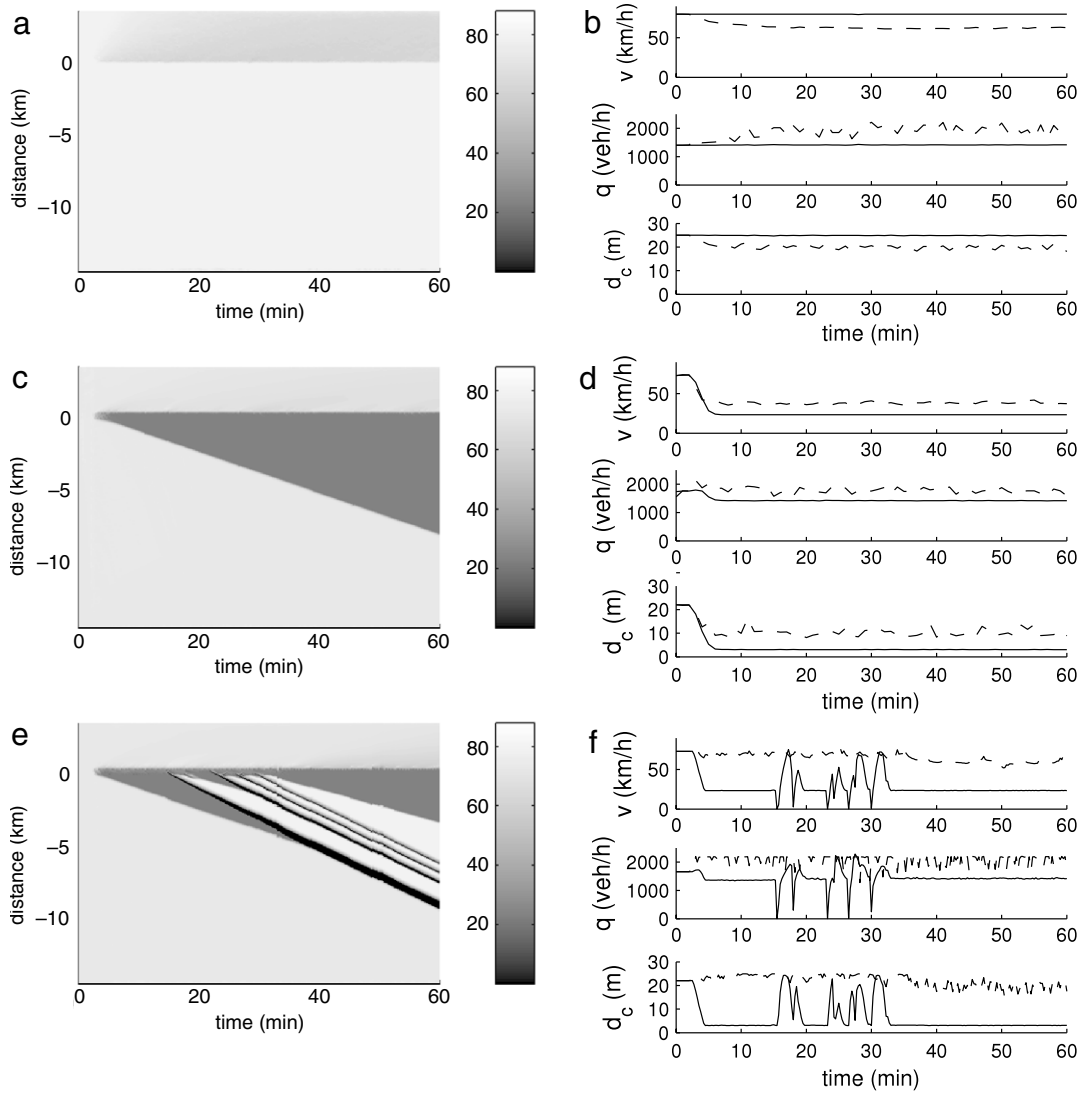

Fig. 6. Spatio-temporal speed diagram and time series of speed, flow rate and d_c at upstream and downstream of an on-ramp. (a), (b): free flow; (c), (d): synchronized flow; (e), (f): wide moving jam. In (b), (d) and (f), solid lines correspond to upstream data and dashed lines downstream data.

5. Explanation of empirical observations

According to the previous empirical analysis and simulation results, it was found that at vicinity of a single on-ramp, there are two effects on the flow: One is the increased flow rate with slightly decrease d_c which is often observed at inhomogeneity downstream caused by lane changes, another is the decreased flow rate with dramatically decreased d_c at inhomogeneity upstream caused by propagated congestion.

In real traffic, flow may be affected by superposition of the above two effects for the dense road inhomogeneities. In Fig. 2, flow-density relations at different sections, even at same section with different lanes, are different from each other. Fig. 7 shows traffic states at 6 sections of a segment of Beijing urban freeway (see Fig. 1) in detail. It is observed that congestion is propagated from section D6 to D3, while congestion at D2 is formed after a spontaneously breakdown at arrow B. The high exit flow to off-ramp R2 is the reason for the separation of the two congestion areas. Then although D2 and D5 are both at immediate on-ramp downstream, their flow-density relations in Fig. 2(b) and (c) are different for the different upstream and downstream situation.

In order to simulate traffic patterns at on-ramp vicinity with different upstream and downstream situations, additional "virtual on-ramps" are settled to simulate merging vehicles at on-ramp upstream and downstream. The road structure used in the simulation is shown in Fig. 8. Besides a real on-ramp, two virtual on-ramps are located at upstream and downstream separately, generating merging vehicles from other lane which affect traffic dynamics at the targeted on-ramp vicinity. By carefully selecting simulation parameters labeled in Fig. 8, some empirical flow-density relations are reproduced well.

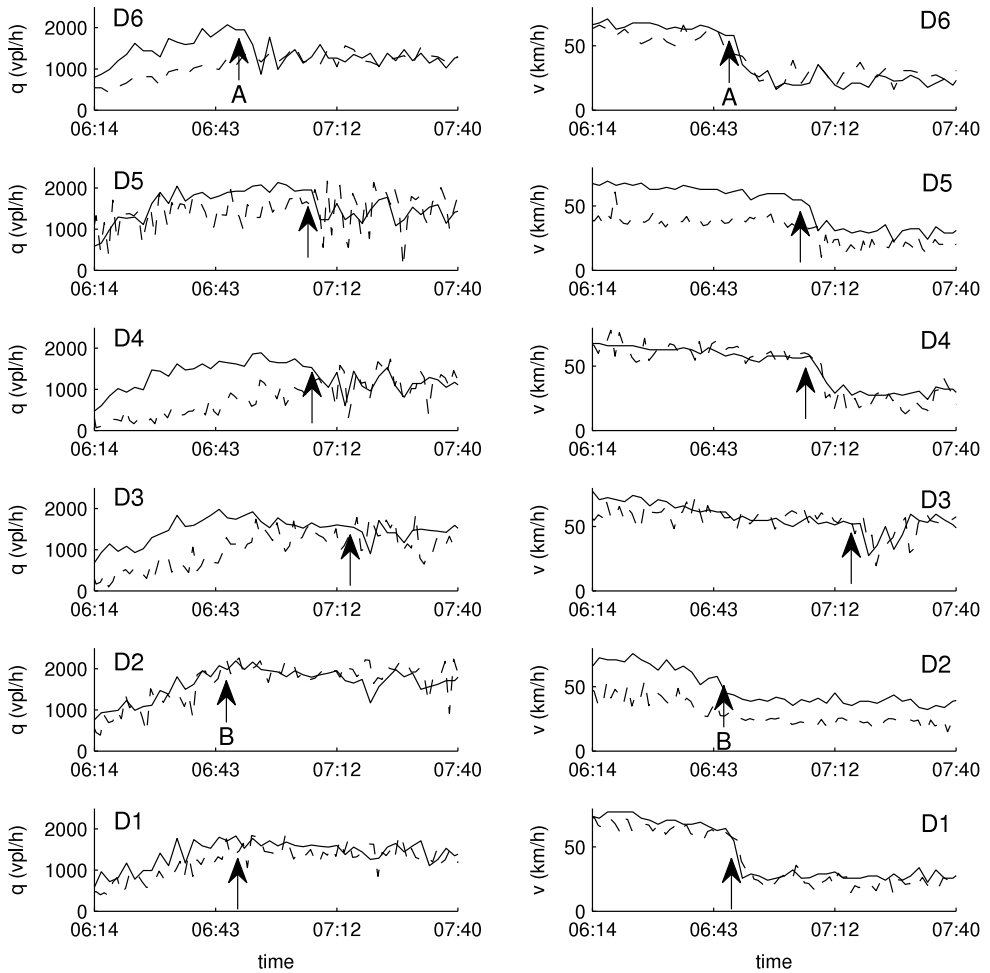

Fig. 7. Empirical traffic 2-min. averaged flow rate and speed at a segment of Beijing urban freeway on a morning peak. Median lane data are indicated with a solid line while the shoulder lane data with a dashed line.

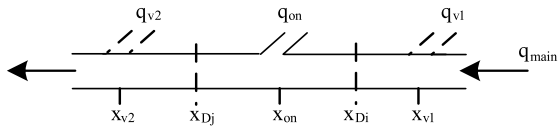

Fig. 8. Simulated one-lane road structure with one on-ramp and two virtual on-ramps. q_{on} are on-ramp flow rate, while q_{v1} and q_{v2} are supposed to be merging flow from other lanes. x_{on} is the on-ramp location. The two virtual on-ramps are settled at x_{v1} and x_{v2}. Average flow rate and density are collected at the location x_{Di} and x_{Dj}, where D_i and D_j correspond to real detectors in Fig. 1. $q_{(main)}$ shows the boundary flows during simulation.

As here only traffic patterns at on-ramp vicinity were considered, median lanes and shoulder lanes at on-ramp vicinities D1, D2, D4 and D5 are selected. The four sections are simulated in four pairs with simulation parameters listed in Table 2. The comparison between empirical data and simulation result are drawn in Fig. 9.

In Fig. 9, most simulation results could represent the empirical data. But deviations are hardly ignored in Fig. 9(c), (g) and (h), where stop-and-go traffic shows different slopes in empirical data and simulated result. This is because the measured data are temporally averaged while simulated result are spatially averaged. The temporally averaged data tend to overestimate speed when vehicles are in frequent acceleration and deceleration. Such that there exist some empirical congested states located at left-bottom of the flow-density plane. In fact, these temporal averaged states correspond to spatio-averaged states located at right-bottom of the flow-density plane. From this point, the empirical data and simulation results are not contrary to each other but qualitatively consistent.

Some simulation parameters in Table 2 are derived from the empirical data, while other parameters such as flow rate of virtual ramps, are derived by analysis. $q_{(main)}$, $d_0^{(down)}$ and $d_0^{(up)}$ are approximated from empirical data. The low $d_0^{(down)}$ appeared at shoulder lane at D2 and D5 is the result of low speed of vehicles from the on-ramps. $q_{(on)}$ at the two shoulder lanes are approximated as real average on-ramp flows at R1 and R4. Since median lane is less affected by on-ramps, $q_{(on)}$ at the two median lanes are less than their corresponding shoulder lanes. $q_{(v1)}$ is used to generate appropriate downstream

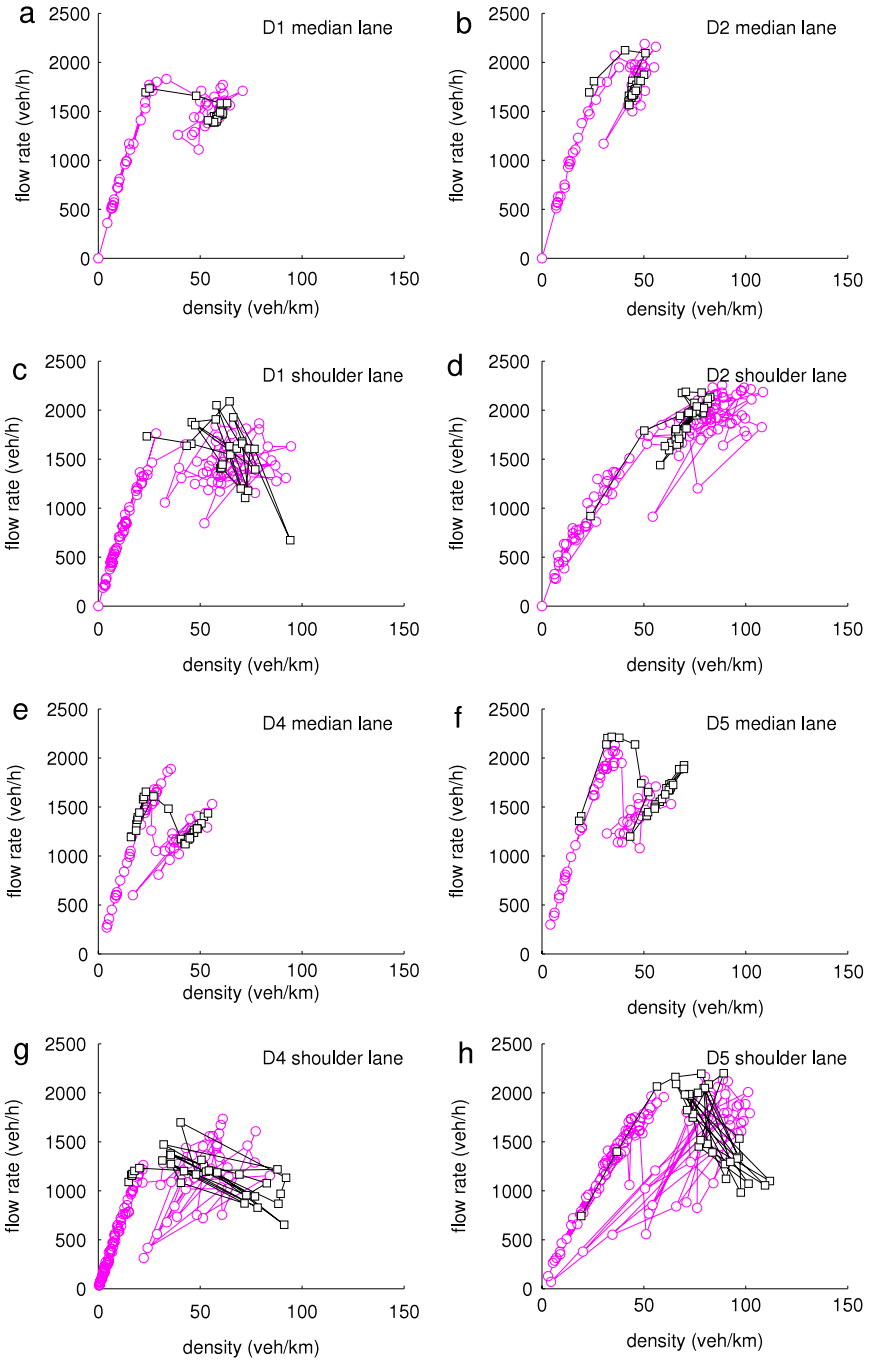

Fig. 9. Comparison between empirical (red circles) and simulated (white squares) 2-min averaged flow-density relations: (a) D1 median lane; (b) D2 median lane; (c) D1 shoulder lane; (d) D2 shoulder lane; (e) D4 median lane; (f) D5 median lane; (g) D4 shoulder lane; (h) D5 shoulder lane. Values of simulation parameters are listed in Table 2.

traffic situation. In pair 3 and pair 4, $q_{(v1)}$ sets to be sufficiently large to generate downstream congestion which follows real traffic situation according to Fig. 7. Since breakdown at D2 is spontaneously formed by local perturbation, $q_{(v1)}$ of pair 1 and pair 2 act as local perturbation which is larger at shoulder lane than at median lane for the high exit flow to off-ramp R2. Similarly, $q_{(v2)}$ is used to generate appropriate upstream traffic situation. In all pairs, $q_{(v2)}$ have no significant deviation.

6. Conclusion

This paper proposes a car-following model based on a multi-branch fundamental diagram in the framework of Kerner's three-phase traffic theory. System features at on-ramp vicinity are investigated by means of computer simulations.

Table 2
Simulation parameters.

	Pair 1: D1/D2 Median lane Fig. 9(a), (b)	Pair 2:D1/D2 Shoulder lane Fig. 9(c), (d)	Pair 3:D4/D5 Median lane Fig. 9(e), (f)	Pair 4:D4/D5 Shoulder lane Fig. 9(g), (h)
$q_{(\text{main})}$ (vpl/h)	1694	1733	1179	1091
$q_{(\text{on})}$ (vpl/h)	420	560	300	780
$q_{(\text{v1})}$ (vpl/h)	120	560	600	520
$q_{(\text{v2})}$ (vpl/h)	60	280	100	0
$d_0^{(\text{up})}$ (m)	22	22	22	22
$d_0^{(\text{down})}$ (m)	22	9	22	9
$d_{\max}^{(\text{up})}$ (m)	25	25	25	25
$d_{\max}^{(\text{down})}$ (m)	25	9	25	9
x_{on} (m)	0	0	0	0
x_{v1} (m)	−225	−225	−350	−350
x_{v2} (m)	225	225	450	450
x_{D1} (m)	0	0	–	–
x_{D2} (m)	300	250	–	–
x_{D4} (m)	–	–	0	−100
x_{D5} (m)	–	–	280	150

Numerical results are consistent with empirical observation on urban freeway. Several conclusions are drawn based on this work:

1. Driver perception to the change of surrounding traffic affects driving behavior, resulting in a non-unique equilibrium velocity at the same gap. The adaption of driving behavior is responsible both for the widely scattered congested traffic states on flow-density plane and the diversity of free flow velocities at different locations.
2. When the surrounding traffic gets congested, drivers tend to drive more cautiously to keep a smooth moving. Such a behavior is simulated by a decreased d_{cr} through a drop of perception distance d_{c}, resulting in a stable flow at a high density with a finite speed, i.e., homogeneous congested flow.
3. When the surrounding traffic has sufficient large changes, the decreased d_{cr} cannot compensate the instability brought by the increasing density, leading to the emergence of moving jams finally.

Acknowledgements

This paper is sponsored by the National Natural Science Foundation (60874078), Program for New Century Excellent Talents in University (NCET-08-0718), Ph.D. Program Foundation of China Ministry of Education (20070004020), National High-Tech R&D Program (2006AA11Z212) and National Basic Research Program of China (2006CB70557).

References

[1] B. Greenshields, A study in highway capacity, in: Proceedings of the Highway Research Board (Highway Research Board), vol. 14, Washington DC, 1935. p. 458.
[2] L. Edie, Following and steady-state theory for non-congested traffic, Oper. Res. 9 (1961) 66–76.
[3] M. Treiber, A. Hennecke, D. Helbing, Congested traffic states in empirical observations and microscopic simulations, Phys. Rev. E, 62 (2), 1805.
[4] K. Nagel, M. Schreckenberg, A cellular automaton model for freeway traffic, J. Phys. I 2 (2) (1992) 2221–2229.
[5] M. Bando, K. Hasebe, A. Nakayama, A. Shibata, Y. Sugiyama, Dynamical model of traffic congestion and numerical simulation, Phys. Rev. E 51 (2) (1995) 1035.
[6] M. Koshi, M. Iwasaki, I. Ohkura, Some findings and an overview on vehicular flow characteristics, in: V. Hurdle, D. Hauer, G. Steuart (Eds.), in: Proceedings of the 8th International Symposium on Transportation and Traffic Theory, Toronto Ontario, 1983, p. 403.
[7] B.S. Kerner, H. Rehborn, Experimental properties of complexity in traffic flow, Phys. Rev. E 53 (5) (1996) R4275.
[8] W. Guan, S. He, Statistical features of traffic flow on urban freeways, Physica A 387 (4) (2008) 944–954.
[9] D. Helbing, D. Batic, M. Schönhof, M. Treiber, Modelling widely scattered states in "synchronized" traffic flow and possible relevance for stock market dynamics, Physica A 303 (1–2) (2002) 251–260.
[10] W. Knospe, L. Santen, A. Schadschneider, M. Schreckenberg, Human behavior as origin of traffic phases, Phys. Rev. E 65 (1) (2001) 015101.
[11] H. Lenz, C.K. Wagner, R. Sollacher, Multi-anticipative car-following model, Eur. Phys. J. B 7 (2) (1999) 331–335.
[12] M. Treiber, D. Helbing, Memory effects in microscopic traffic models and wide scattering in flow-density data, Phys. Rev. E 68 (4) (2003) 046119.
[13] M. Treiber, A. Kesting, D. Helbing, Understanding widely scattered traffic flows, the capacity drop, and platoons as effects of variance-driven time gaps, Phys. Rev. E 74 (1) (2006) 016123.
[14] M.E. Fukui, Y. Sugiyama, M. Schreckenberg, D. Wolf (Eds.), Traffic and Granular Flow'01, Springer, 2003.
[15] C.F. Daganzo, A behavioral theory of multi-lane traffic flow. part i: Long homogeneous freeway sections, Transp. Res., Part B: Methodol. 36 (2) (2002) 131–158.
[16] J.A. Laval, L. Leclercq, Microscopic modeling of the relaxation phenomenon using a macroscopic lane-changing model, Transp. Res., Part B: Methodol. 42 (6) (2008) 511–522.
[17] T. Forbes, Human factor considerations in traffic flow theory, Highway Res. Record 15 (1963) 60–66.
[18] R. Nagai, T. Nagatani, A. Yamada, Phase diagram in multi-phase traffic model, Physica A 355 (2–4) (2005) 530–550.
[19] H. Zhang, T. Kim, A car-following theory for multiphase vehicular traffic flow, Transp. Res., Part B: Methodol. 39 (2005) 385–399.
[20] F. Siebel, W. Mauser, Synchronized flow and wide moving jams from balanced vehicular traffic, Phys. Rev. E 73 (6) (2006) 066108–066110.

[21] B.S. Kerner, The Physics of Traffic: Empirical Freeway Pattern Features, Engineering Applications and Theory, Springer, 2004.
[22] B.S. Kerner, S.L. Klenov, Deterministic microscopic three-phase traffic flow models, J. Phys. A: Math. General 39 (8) (2006) 1775–1809.
[23] S. He, W. Guan, Empirical investigation on phase diagram at urban freeway with on-ramp, in: The 11th International IEEE Conference on Intelligent Transportation Systems, 2008, pp. 880–887.
[24] D. Helbing, B.A. Huberman, Coherent moving states in highway traffic, Nature 396 (24) (1998) 738–740.
[25] W. Guan, S. He, Phase transition of urban freeway traffic flow, in: Proceedings of IEEE International Conference on Intelligence Transportation System, Beijing, 2008, pp. 868–874.